MOMENTUM DISTRIBUTION AND THE MEAN FREE PATH OF NUCLEONS IN NUCLEAR MATTER*

By J. Dąbrowski

Institute for Nuclear Studies, Warsaw**

(Received March 12, 1986)

Realistic momentum distribution in nuclear matter is used in calculating the absorptive potential W and the nucleon mean free path λ for nucleon energies $e \lesssim 200$ MeV. W is calculated with a simple expression in terms of free NN cross section, which takes care of Pauli blocking and binding effects. Whereas previous calculations suggested a sharp increase in λ as $e \to 0$, present results show a much smoother dependence of λ on e, with $\lambda = 5 \pm 1$ fm in the whole energy range $0 \lesssim e \lesssim 200$ MeV.

PACS numbers: 21.65.+f

1. Introduction

The mean free path λ of a nucleon in nuclear matter is one of the fundamental characteristics of nuclear matter. Directly related to λ is the imaginary part W of the nuclear optical potential ($W \sim 1/\lambda$). A simple expression for λ (and W) in terms of the free total NN cross section was derived in [1] (hereafter referred to as I). Its application led to a reasonable agreement with the experimental estimates for nucleon energies $e \sim 50$–200 MeV. On the other hand, λ calculated in I for $e \lesssim 50$ MeV turned out to be too big as compared with experimental estimates. One obvious reason for this failure was the use in I for $n(k_N)$, the distribution of nucleon momenta k_N in nuclear matter (i.e., the probability that the k_N state is occupied), the step function

$$n(k_N) = n_0(k_N) = \theta(k_F - k_N), \tag{1.1}$$

where k_F is the Fermi momentum in nuclear matter (all momenta are measured in units of $\hbar$). Namely, if we consider a nucleon moving with momentum k_0 in nuclear matter with momentum distribution $n = n_0$, we get

$$W \to 0, \quad \lambda \to \infty \quad \text{for} \quad k_0 \to k_F, \tag{1.2}$$

* Research supported by the Polish-U.S. Maria Skłodowska-Curie Fund under Grant No P-F7F037P.

** Address: Instytut Problemów Jądrowych, Hoża 69, 00-681 Warszawa, Poland.

because of the complete Pauli blocking at $k_0 = k_F$. As a consequence of (1.2), we get very small values of $|W(k_0)|$ and very big values of $\lambda(k_0)$ for $k_0 \gtrsim k_F$. If we replace n_0 by a realistic diffused distribution n, $W(k_F) \neq 0$ and $\lambda(k_F)$ is finite, because now the Pauli blocking is not complete even at $k_0 = k_F$. Consequently, $|W(k_0)|$ increases and $\lambda(k_0)$ decreases for $k_0 \gtrsim k_F$.

In the present paper W and λ are calculated as in I, however $n_0(k_N)$ used in I is replaced by a realistic distribution $n(k_N)$ determined by Fantoni and Pandharipande [2]. At low nucleon energies, results obtained for W and in particular for λ change markedly because of this replacement, and agree with existing experimental estimates better than the results of I.

In Section 2, we outline the derivation of the expressions for W, λ, and the equivalent local potential W_L. In Section 3, we present our results for W_L and λ, and compare them with experiment. Formulae used in computing W are presented in Appendix.

2. *Expressions for W and λ*

Replacing the distribution n_0 by n in the procedure of I, although simple in principle, requires some care. For this reason, we briefly outline the derivation of the expressions for W and λ, presented in detail in I, with n_0 replaced by n.

Our starting expression for the absorptive potential of a nucleon "0" moving with momentum $\boldsymbol{k}_0$ through symmetric ($N = Z$) nuclear matter of density ϱ is:

$$W(k_0) = 4(2\pi)^{-3} \int d\boldsymbol{k}_1 n(k_1) \operatorname{Im} \langle \boldsymbol{k}|\mathscr{K}|\boldsymbol{k}\rangle, \tag{2.1}$$

where $\boldsymbol{k}_1$ is the momentum of the nucleon "1" of nuclear matter,

$$\boldsymbol{k} = (\boldsymbol{k}_0 - \boldsymbol{k}_1)/2 \tag{2.2}$$

is the "0"–"1" relative momentum. The factor 4 takes care of the four spin-isospin states of a given momentum $\boldsymbol{k}_1$ — otherwise spin and isospin is suppressed in our notation.

The reaction matrix $\mathscr{K}$ is defined by

$$\mathscr{K} = v + v[Q/(\alpha + i\eta)]\mathscr{K}, \tag{2.3}$$

where v is the NN potential,

$$Q = Q(k_1', k_0') = [1 - n(k_1')]\,[1 - n(k_0')] \tag{2.4}$$

is the exclusion principle operator,

$$\alpha = e(k_1) + e(k_0) - e(k_1') - e(k_0'), \tag{2.5}$$

and k_0', k_1' are nucleon momenta in the intermediate states.

The single particle (s.p.) energy $e(k_N)$ of a nucleon with momentum k_N is assumed in the form:

$$e(k_N) = \begin{cases} \varepsilon(k_N)/\mu + D & \text{for} \quad k_N < k_F, \\ \varepsilon(k_N)/\nu + C & \text{for} \quad k_N > k_F, \end{cases} \tag{2.6}$$

where $\varepsilon(k_N) = \hbar^2 k_N^2/2M$, and the ratio of the effective to the real nucleon mass, M^*/M, is denoted by μ for $k_N < k_F$ and by ν for $k_N > k_F$. The constants μ, ν, D, and C, which depend on ϱ, are determined as in I.

Eq. (2.3) implies the optical theorem:

$$\begin{aligned} \operatorname{Im}\langle \boldsymbol{k}|\mathscr{K}|\boldsymbol{k}\rangle &= -\tfrac{1}{2}(2\pi)^{-2}\int d\boldsymbol{k}' Q|\langle \boldsymbol{k}'|\mathscr{K}|\boldsymbol{k}\rangle|^2\delta(\alpha) \\ &= -2(\hbar^2/M)k\int d\hat{k}'(d\sigma^{\mathrm{NM}}/d\hat{k}')\int dk' k' Q\delta(\alpha) \\ &\cong -2(\hbar^2/M)k\bar{\sigma}(4\pi)^{-1}\int d\hat{k}'\int dk' k' Q\delta(\alpha), \end{aligned} \tag{2.7}$$

where

$$\boldsymbol{k}' = (\boldsymbol{k}_0' - \boldsymbol{k}_1')/2 \tag{2.8}$$

is the relative momentum in the intermediate state.

In the second step in Eq. (2.7), we introduce the differential NN cross section (in the CM system) in nuclear matter,

$$d\sigma^{\mathrm{NM}}/d\hat{k}' = (k'/k)\,(M/4\pi\hbar^2)^2|\langle \boldsymbol{k}'|\mathscr{K}|\boldsymbol{k}\rangle|^2, \tag{2.9}$$

in which k' is determined by the energy conservation equation, $\alpha = 0$.

In the last step in Eq. (2.7), we make the crucial approximation:

$$d\sigma^{\mathrm{NM}}/d\hat{k}' \cong \bar{\sigma}/4\pi = \tfrac{1}{2}(\sigma_{nn}+\sigma_{np})/4\pi, \tag{2.10}$$

i.e., we approximate the NN cross section in nuclear matter by the average total NN cross section for free NN scattering (σ_{nn} and σ_{np} are total cross sections for nn and np scattering). The approximate treatment of the $\hat{k}'$ integration in the last step in Eq. (2.7) means that we replace $Q\delta$ by its angle average.

By inserting expression (2.7) into Eq. (2.1), we get our final result for $W(k_0)$:

$$W(k_0) = -8(\hbar^2/M)^2(2\pi)^{-3}\int d\boldsymbol{k}_1 n(k_1)k\bar{\sigma}(4\pi)^{-1}\int d\hat{k}'\int dk' k' Q\delta(\alpha). \tag{2.11}$$

Let us denote by W_0 the value of W in the case of $n = n_0$. Only states with $k_0' > k_F$, $k_1' > k_F$ contribute to W_0. For these states $\alpha = -\hbar^2 k'^2/M\nu +$ terms independent of k', and the integration over $\hat{k}'$ and k' in (2.11) can be performed analytically with the result

$$W_0(k_0) = -4\hbar^2\nu(2\pi)^{-3}\int^{<k_F} d\boldsymbol{k}_1 \bar{Q}\bar{\sigma}k/M, \tag{2.12}$$

where $\bar{Q}$ is the angle average of Q (expressions for $\bar{Q}$ are given in Eqs. (B.5a–b) of I). In the case of $n \neq n_0$, an analytical integration over $\hat{k}'$ is impossible even for the states with $k_0' > k_F$, $k_1 > k_F$. Furthermore, when $n \neq n_0$ there are other states that contribute to W, e.g., those with $k_1' < k_F$, $k_0' > k_F$. For those states α depends not only on k' but also on x', the cosine of the angle between $\boldsymbol{k}'$ and the total conserved momentum of the two nucleons "0" and "1",

$$\boldsymbol{K} = \boldsymbol{k}_0 + \boldsymbol{k}_1 = \boldsymbol{k}_0' + \boldsymbol{k}_1', \tag{2.13}$$

and this complicates further the calculation of W.

where $\varepsilon(k_N) = \hbar^2 k_N^2/2M$, and the ratio of the effective to the real nucleon mass, M^*/M, is denoted by μ for $k_N < k_F$ and by ν for $k_N > k_F$. The constants μ, ν, D, and C, which depend on ϱ, are determined as in I.

Eq. (2.3) implies the optical theorem:

$$\begin{aligned} \mathrm{Im}\,\langle \boldsymbol{k}|\mathscr{K}|\boldsymbol{k}\rangle &= -\tfrac{1}{2}(2\pi)^{-2}\int d\boldsymbol{k}' Q|\langle \boldsymbol{k}'|\mathscr{K}|\boldsymbol{k}\rangle|^2\delta(\alpha) \\ &= -2(\hbar^2/M)k\int d\hat{k}'(d\sigma^{NM}/d\hat{k}')\int dk' k' Q\delta(\alpha) \\ &\cong -2(\hbar^2/M)k\bar{\sigma}(4\pi)^{-1}\int d\hat{k}'\int dk' k' Q\delta(\alpha), \end{aligned} \tag{2.7}$$

where

$$\boldsymbol{k}' = (\boldsymbol{k}_0' - \boldsymbol{k}_1')/2 \tag{2.8}$$

is the relative momentum in the intermediate state.

In the second step in Eq. (2.7), we introduce the differential NN cross section (in the CM system) in nuclear matter,

$$d\sigma^{NM}/d\hat{k}' = (k'/k)\,(M/4\pi\hbar^2)^2|\langle \boldsymbol{k}'|\mathscr{K}|\boldsymbol{k}\rangle|^2, \tag{2.9}$$

in which k' is determined by the energy conservation equation, $\alpha = 0$.

In the last step in Eq. (2.7), we make the crucial approximation:

$$d\sigma^{NM}/d\hat{k}' \cong \bar{\sigma}/4\pi = \tfrac{1}{2}(\sigma_{nn}+\sigma_{np})/4\pi, \tag{2.10}$$

i.e., we approximate the NN cross section in nuclear matter by the average total NN cross section for free NN scattering (σ_{nn} and σ_{np} are total cross sections for nn and np scattering). The approximate treatment of the $\hat{k}'$ integration in the last step in Eq. (2.7) means that we replace $Q\delta$ by its angle average.

By inserting expression (2.7) into Eq. (2.1), we get our final result for $W(k_0)$:

$$W(k_0) = -8(\hbar^2/M)^2(2\pi)^{-3}\int d\boldsymbol{k}_1 n(k_1) k\bar{\sigma}(4\pi)^{-1}\int d\hat{k}'\int dk' k' Q\delta(\alpha). \tag{2.11}$$

Let us denote by W_0 the value of W in the case of $n = n_0$. Only states with $k_0' > k_F$, $k_1' > k_F$ contribute to W_0. For these states $\alpha = -\hbar^2 k'^2/Mv +$ terms independent of k', and the integration over $\hat{k}'$ and k' in (2.11) can be performed analytically with the result

$$W_0(k_0) = -4\hbar^2 v(2\pi)^{-3}\int^{<k_F} d\boldsymbol{k}_1 \bar{Q}\bar{\sigma}k/M, \tag{2.12}$$

where $\bar{Q}$ is the angle average of Q (expressions for $\bar{Q}$ are given in Eqs. (B.5a–b) of I). In the case of $n \neq n_0$, an analytical integration over $\hat{k}'$ is impossible even for the states with $k_0' > k_F$, $k_1 > k_F$. Furthermore, when $n \neq n_0$ there are other states that contribute to W, e.g., those with $k_1' < k_F$, $k_0' > k_F$. For those states α depends not only on k' but also on x', the cosine of the angle between $\boldsymbol{k}'$ and the total conserved momentum of the two nucleons "0" and "1",

$$\boldsymbol{K} = \boldsymbol{k}_0 + \boldsymbol{k}_1 = \boldsymbol{k}_0' + \boldsymbol{k}_1', \tag{2.13}$$

and this complicates further the calculation of W.

As the equilibrium density of nuclear matter we use the value $\varrho_0 = 0.160\,\mathrm{fm}^{-3}$ ($k_{F0} = 1.33\,\mathrm{fm}^{-1}$), used in [2]. It differs slightly from the value of $\varrho_0 = 0.166\,\mathrm{fm}^{-3}$ ($k_{F0} = 1.35\,\mathrm{fm}^{-1}$) used in I. Consequently, values of the parameters of the s.p. potential, Eq. (2.6), differ slightly from those used in I. The present values, determined as described in I (with the volume energy of nuclear matter $\varepsilon_{vol} = -15.8$ MeV), are: $D(\varrho_0) = -110$ MeV, $C(\varrho_0) = -68$ MeV, $v(\varrho_0) = 0.7$, $\mu(\varrho_0) = 0.4$, and $D(\varrho_0/2) = -66$ MeV, $C(\varrho_0/2) = -48$ MeV, $v(\varrho_0/2) = 0.8$, $\mu(\varrho_0/2) = 0.5$.

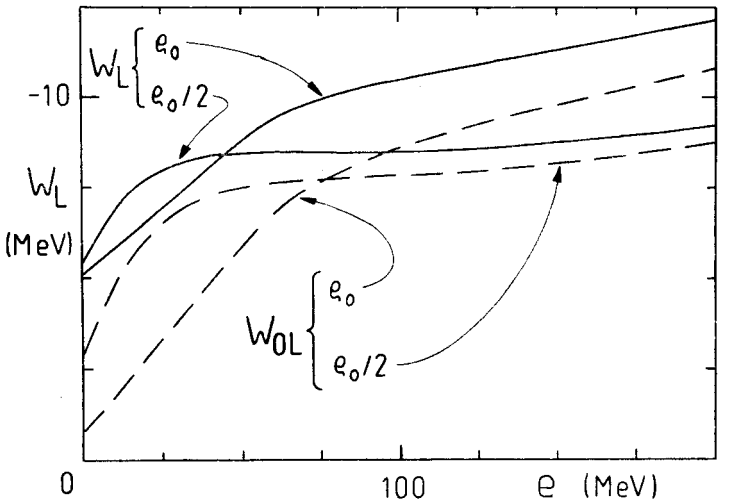

Fig. 2. $W_L(e)$ and $W_{0L}(e)$ calculated at $\varrho = \varrho_0$ and $\varrho = \varrho_0/2$

For $\bar{\sigma}$ we use the same parametrization as in I, fitted to the np and nn experimental cross sections.

Results obtained for W_L and λ are presented as functions of the energy e, connected with k_0 by Eq. (2.6). This enables us to compare our results directly with experiment.

The equivalent local absorptive potential as a function of the nucleon (neutron) energy, $W_L(e)$, calculated with the distribution n at $\varrho = \varrho_0$ and $\varrho = \varrho_0/2$ is shown in Fig. 2. For comparison, we also show in Fig. 2 the equivalent potential W_{0L}, calculated with the distribution n_0. Replacing n_0 by the realistic distribution n increases $|W_L|$, especially at low energies. This increase, more pronounced at ϱ_0 than at $\varrho_0/2$, is caused by the weakening of the Pauli blocking. Comparing the results for ϱ_0 and $\varrho_0/2$, we notice that at low energies $|W_L(\varrho_0)| < |W_L(\varrho_0/2)|$ and at high energies $|W_L(\varrho_0)| > |W_L(\varrho_0/2)|$, which reflects the decreasing role of the Pauli blocking with the increasing energy. This explains the observed surface peaking of the absorptive optical potential at low energies, and the volume type absorption at higher energies. Since the effect is the result of the Pauli blocking, it is more pronounced in the case of the distribution n_0 than in the case of n.

The space of k_1, k_1', k_0' may be divided into the following six regions: (Ai) $k_1' < k_F$, $k_0' < k_F$; (Bi) $k_1' > k_F$, $k_0' > k_F$; (Ci) $k_1' > k_F$, $k_0' < k_F$ or $k_1' < k_F$, $k_0' > k_F$, where $k_i < k_F$ for $i = 1$, and $k_i > k_F$ for $i = 2$. The contributions of these regions to W_L and their sum

W_L(TOT) are shown in Fig. 3. Energy and momentum conservation does not allow real scattering $k_0 k_1 \to k_0' k_1'$ to occur in region A2, and consequently $W_L(A2) = 0$. Similarly $W_L(A1) = 0$ for $e \gtrsim 15$ MeV, and $|W_L(A1)|$ for $r \lesssim 15$ MeV is too small to be visible in Fig. 3. Most important at higher energies is the region B1 (the only region which contributes to W_{0L}). As $k_0 \to k_F$ ($e \to -15.8$ MeV), the number of states in this region, compatible with energy and momentum conservation, shrinks to zero. Consequently, at sufficiently low energies $|W_L(B1)|$ becomes small compared to other contributions, especially

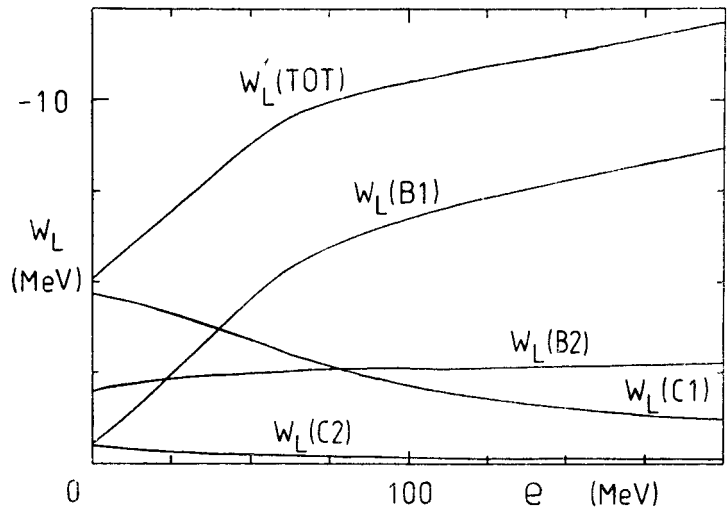

Fig. 3. Different contributions to W_L at $\varrho = \varrho_0$

$|W_L(C1)|$. Of course, the actual magnitude of the contributions depends also on the cross section $\bar{\sigma}$ which increases sharply with decreasing relative momentum k.

Fig. 4 shows the results for the mean free path λ as a function of e, obtained with the realistic distribution n at $\varrho = \varrho_0$ and $\varrho = \varrho_0/2$. Results for the mean free path λ_0, obtained with the distribution n_0, are also shown in Fig. 4. At high energies, λ is only slightly smaller than λ_0. As the energy e diminishes, λ does not change very much whereas λ_0, especially at $\varrho = \varrho_0$, increases rapidly as $e \to 0$. Notice also that at low energies the density dependence of λ is much weaker than that of λ_0: $\lambda(\varrho_0)$ is only slightly bigger than $\lambda(\varrho_0/2)$ whereas $\lambda_0(\varrho_0) \gg \lambda_0(\varrho_0/2)$. In short, our results indicate that the mean free path does not depend on energy and density so drastically as the $n = n_0$ results suggest.

In Fig. 5, our results for W_L and W_{0L} are compared with a sample of empirical estimates of the central depth of the imaginary part of the phenomenological local optical potential. Full circles are neutron–heavy nuclei data from the early compilation of Hodgson (p. 87 of [7]), open circles are from the compilation of Bohr and Mottelson (p. 237 of [8]), and crosses are from recent proton scattering on ^{208}Pb and ^{40}Ca (Nadasen et al. [9]; to obtain the corresponding neutron energy e from the proton energy e_p, the Coulomb and symmetry correction was used as in I). The comparison of our results with empirical estimates is inconclusive. Especially at low energy, where the effect of a realistic momentum distribution

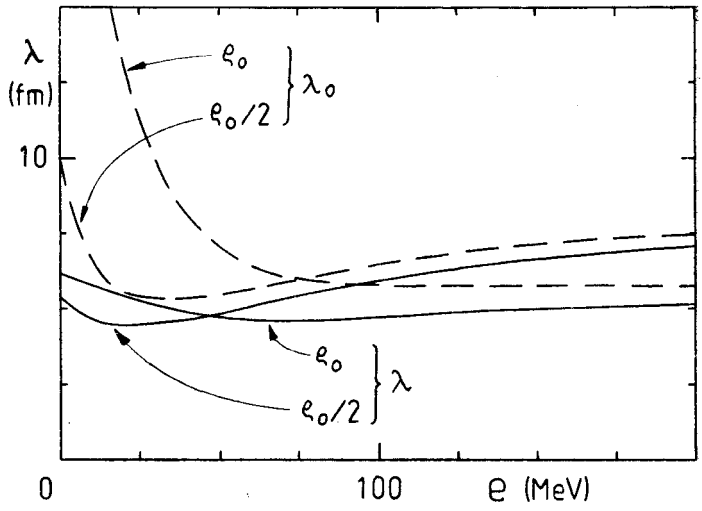

Fig. 4. $\lambda(e)$ and $\lambda_0(e)$ calculated at $\varrho = \varrho_0$ and $\varrho = \varrho_0/2$

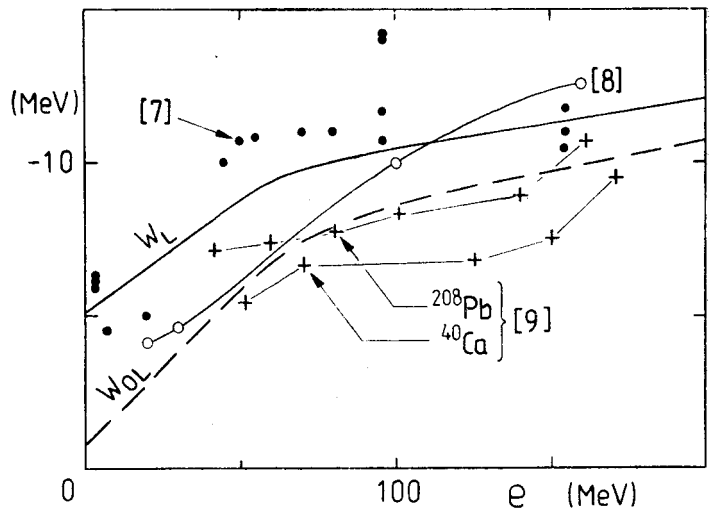

Fig. 5. $W_L(e)$ and $W_{0L}(e)$ calculated at $\varrho = \varrho_0$ compared with empirical estimates

is biggest, the depth of the phenomenological absorptive potential in the central part of heavy nuclei is not well determined because of the strong surface absorption, and also the presence of compound-elastic scattering. But also at higher energies, there are problems with the phenomenological depth of W_L, recently pointed out by Meyer and Schwandt [10] (noticed already by Elton [11]). There are theoretical reasons (see, e.g., [12]) to believe that at higher energies the real part of the optical potential acquires a wine-bottle shape which, in turn, affects the depth of W_L. For example, the analysis of $^{40}Ca(\vec{p}, p)^{40}Ca$ elastic scattering at $e_p = 180$ MeV ($e \cong 170$ MeV) suggests the value of $W_L \cong 25$ MeV [10],

which is much bigger than all the values (obtained with a standard shape of the real potential) shown in Fig. 5.

In Fig. 6, our results for λ and λ_0 are compared with empirical estimates. The results of Ref. [8] and the Ca, Pb results of Ref. [9] were obtained from the corresponding results for W_L in Fig. 5 by applying Eq. (2.6). In the same way, the horizontally shaded band is obtained from the results for W_L of Ref. [10] (based on a real potential of a wine-bottle shape). The vertically shaded band denotes the range of λ values determined in Ref. [9] from p — ^{40}C reaction cross section. The result of Ref. [13] is an estimated upper limit

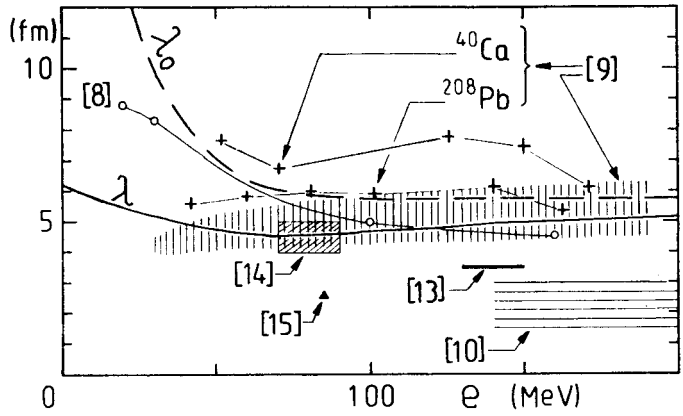

Fig. 6. $\lambda(e)$ and $\lambda_0(e)$ calculated at $\varrho = \varrho_0$ compared with empirical estimates

of λ inferred from inclusive proton-induced spectra. The estimate of [14] was obtained by fitting λ to angle integrated proton singles spectrum in (p, x) experiments. (The lower energy limits of the estimates of [10], [13], and [14] shown in Fig. 6 stem from subtracting Coulomb and symmetry energy from experimental energies e_p to get e.) The estimate [15] is the result of adjusting the collision term in describing heavy ion collisions.

The agreement (or disagreement) of our results for the mean free path with the experimental results obtained from the empirical imaginary optical potential, via relation (2.6), simply reflects the situation with W_L in Fig. 5. In general, our results for λ agree better with the other experimental estimates (obtained not from empirical values of W_L). The best agreement is achieved with the results of the recent proton reaction cross section measurement by Nadasen et al. [9] (and also with the less direct estimate of [14]). Inspite of the considerable spread of the empirical points in Fig. 6, none of them for $e \lesssim 50$ MeV is compatible with our results for λ_0 which increases rapidly with decreasing energy. In this respect, all the experimental results favour the mean free path λ calculated with the realistic momentum distribution. Our results suggest that $\lambda = 5 \pm 1$ fm in the whole energy range considered, $0 \lesssim e \lesssim 200$ MeV.

All the numerical computations were performed on the Olivetti M21 Personal Computer, and the author thanks Dr. Jacek Rożynek for his expert help in subduing the computer.

APPENDIX

Computation of $W(k_0)$

Here, as in actual computations, we introduce $\tilde{k}_N = k_N/k_F$. However, to simplify our formulae, we drop the tilde in our notation. This means, that in the Appendix (and only here) k_N denotes the momentum measured in units of the Fermi momentum.

In the new notation, Eq. (2.11) (with the help of formula (3.16) of I) takes the form:

$$W(k_0) = -(N/k_0)\int_0^\infty dk_1 n(k_1)\int_{\gamma(-)}^{\gamma(+)} dk k^2\bar{\sigma}(k)\,\tfrac{1}{2}\int_{-1}^{1} dx'\int_0^\infty dk' k' Q(k_1', k_0')\delta(\alpha), \tag{A.1}$$

where $N = (32/\pi^2)\varepsilon_F^2 k_F^2$, $\varepsilon_F = \hbar^2 k_F^2/2M$, $\gamma(\pm) = |k_0 \pm k_1|/2$, $x' = \hat{k}'\hat{K}'$. The momenta k_0' and k_1' are determined by K, k', and x':

$$\left.\begin{matrix} k_0' \\ k_1' \end{matrix}\right\} = [(K/2)^2 + k'^2 \pm Kk'x']^{1/2}. \tag{A.2}$$

Furthermore,

$$K = 2[(k_1^2 + k_0^2)/2 - k^2]^{1/2}. \tag{A.3}$$

The contributions $W(\mathrm{Y}i)$ of each of the k_1, k_1', k_0' regions $\mathrm{Y}i$ (Y = A, B, C and i = 1, 2) defined in Section 3, are calculated separately. Notice that we always have $k_0 > 1$.

To simplify computations, we introduce the following quantities:

$$n_\alpha(k_N) = \begin{cases} n(k_N) \\ \\ 1 \end{cases} \qquad n(k_N)_\beta = \begin{cases} 1 & \text{for} \quad k_N < 1, \\ \\ n(k_N) & \text{for} \quad k_N > 1, \end{cases} \tag{A.4}$$

$$Q_{yz}(K, k', x') = [1 - n_y(k_1')]\,[1 - n_z(k_0')], \tag{A.5}$$

where y and z stand for α or β, and where the connection between k_1', k_0' and K, k', x' is given in (A.2).

We outline our procedure in the case of region A1. We have:

$$W(\mathrm{A1}) = -(N/k_0)\int_0^1 dk_1 k_1 n(k_1)\int_{\gamma(-)}^{\gamma(+)} dk k^2\bar{\sigma}(k)\,\tfrac{1}{2}\int_{-1}^{1} dx'\int_0^\infty dk' k' Q_{\alpha\alpha}(K, k', x')\delta(\alpha_{\mathrm{A1}}), \tag{A.6}$$

where α_{A1} is the value of α, Eq. (2.5), in region A1:

$$\begin{aligned} \alpha_{\mathrm{A1}}/\varepsilon_F &= k_0^2/\nu + k_1^2/\mu - k_0'^2/\mu - k_1'^2/\mu + (C-D)/\varepsilon_F \\ &= -(1/\mu - 1/\nu)(k_0^2 - 1) + (2/\mu)(k^2 - k'^2). \end{aligned} \tag{A.7}$$

In the last step in Eq. (A.7), we use Eqs (A.2–3) and the relation $(C-D)/\varepsilon_F = 1/\mu - 1/\nu$ which follows from the continuity of $e(k_N)$ at $k_N = 1$.

To perform the k' integration in (A.6), we use the formula:

$$\int_0^\infty dk'k'Q_{\alpha\alpha}\delta(\alpha_{A1}) = \sum \{k'Q_{\alpha\alpha}(K, k', x')/|d\alpha_{A1}/dk'|\}_{k'=k'_{A1}}, \tag{A.8}$$

where the sum extends over all positive solutions k'_{A1} of the energy conservation equation, $\alpha_{A1} = 0$. As is seen from Eq. (A.7), there is only one such solution,

$$k'_{A1} \cong [k^2-(1-\mu/v)(k_0^2-1)/2]^{1/2}, \tag{A.9}$$

and we get

$$W(A1)/\varepsilon_F = -(8k_F^2\mu/\pi^2k_0)\int_0^1 dk_1k_1n(k_1)\int_{\gamma(-)}^{\gamma(+)} dkk^2\bar{\sigma}(k)\bar{Q}_{\alpha\alpha}(K, k'_{A1}), \tag{A.10}$$

where

$$\bar{Q}_{\alpha\alpha}(K, k'_{A1}) = \tfrac{1}{2}\int_{-1}^1 dx'Q_{\alpha\alpha}(K, k'_{A1}, x'). \tag{A.11}$$

Following the same procedure in region A2 we find that $W(A2) = 0$, and the results in the remaining regions are (we use the notation: $a(1) = 0$, $b(1) = 1$, $a(2) = 1$, $b(2) = \infty$):

$$W(Bi)/\varepsilon_F = -(8k_F^2v/\pi^2k_0)\int_{a(i)}^{b(i)} dk_1k_1n(k_1)\int_{\gamma(-)}^{\gamma(+)} dkk^2\bar{\sigma}(k)\bar{Q}_{\beta\beta}(K, k'_{Bi}), \tag{A.12}$$

where

$$\bar{Q}_{\beta\beta}(K, k'_{Bi}) = \tfrac{1}{2}\int_{-1}^1 dx'Q_{\beta\beta}(K, k'_{Bi}, x'), \tag{A.13}$$

$$k'_{B1} = [k^2-(v/\mu-1)(1-k_1^2)]^{1/2}, \quad k'_{B2} = k, \tag{A.14}$$

and

$$W(Ci)/\varepsilon_F = -(16k_F^2\{2\mu v/[v+\mu]\}/\pi^2k_0) \times \int_{a(i)}^{b(i)} dk_1n(k_1)\int_{\gamma(-)}^{\gamma(+)} dkk^2\bar{\sigma}(k)\tilde{Q}_{\alpha\beta}(K, k'_{Ci}), \tag{A.15}$$

where

$$\tilde{Q}_{\alpha\beta}(K, k'_{Ci}) = \tfrac{1}{2}\int_{-1}^1 dx'Q_{\alpha\beta}(K, k'_{Ci})k'_{Ci}/|k'_{Ci}-\tfrac{1}{2}[(v-\mu)/(v+\mu)]Kx'|, \tag{A.16}$$

$$k'_{Ci} = \tfrac{1}{2}(v+\mu)^{-1}[(v-\mu)Kx'+\{[(v-\mu)Kx']^2+4(v+\mu)\xi_i\}^{1/2}], \tag{A.17}$$

where

$$\xi_1 = \mu[k_0^2-(K/2)^2]+v[k_1^2-(K/2)^2],$$

$$\xi_2 = \mu[k_0^2+k_1^2-(K/2)^2-1]+v[1-(K/2)^2]. \tag{A.18}$$

Whenever it happens that for a certain range of k_1, k, x' the expression for k'_{Yi} contains a square root of a negative quantity, it means that the corresponding energy conservation

equation $\alpha_{Yi} = 0$ has no real solution, i.e., a real scattering is not possible. Consequently this range of k_1, k, x' gives zero contribution to $W(Yi)$. (For this reason the lower limit -1 in the x' integration in (A.16) may be replaced by 0. This is also the reason for which $W(A2) = 0$.)

To get the total W, one has to add all the contributions,

$$W = W(A1) + \sum_{i=1}^{2} \{W(Bi) + W(Ci)\}. \tag{A.19}$$

In the case of $n = n_0$, $W = W(B1)$ and $\bar{Q}_{\beta\beta}(K, k') \equiv Q(K, k')$ (expressions for $Q(K, k')$ are given in Eqs (B.5a–b)). The resulting expression for W coincides with the one used in I.

REFERENCES

[1] J. Dąbrowski, W. Piechocki, *Acta Phys. Pol.* **B16**, 1095 (1985).
[2] S. Fantoni, V. R. Pandharipande, *Nucl. Phys.* **A427**, 473 (1984).
[3] S. Fantoni, B. L. Friman, V. R. Pandharipande, *Phys. Lett.* **104B**, 89 (1981).
[4] J. W. Negele, K. Yazaki, *Phys. Rev. Lett.* **47**, 71 (1981).
[5] J. W. Negele, *Comments Nucl. Part. Phys.* **12**, 1 (1983).
[6] I. E. Legaris, V. R. Pandharipande, *Nucl. Phys.* **A235**, 349 (1981).
[7] P. E. Hodgson, *The Optical Model of Elastic Scattering*, Clarendon Press 1963.
[8] A. Bohr, B. Mottelson, *Nuclear Structure*, Vol. I, W. A. Benjamin Inc. 1969.
[9] A. Nadasen, P. Schwandt, P. P. Singh, W. W. Jacobs, A. D. Bacher, P. T. Debevec, M. D. Kaitchuck, J. T. Meek, *Phys. Rev.* **C23**, 1023 (1981).
[10] H. O. Meyer, P. Schwandt, *Phys. Lett.* **107B**, 353 (1981).
[11] L. R. B. Elton, *Nucl. Phys.* **89**, 69 (1966).
[12] P. Scwandt, Proceedings of the Symposium on Light Ion Reaction Mechanisms, RCNP Osaka, May 16–20, 1983, p. 3.
[13] R. E. Segel, S. M. Levenson, P. Żuprański, A. A. Hassan, S. Mukhopadhyay, *Phys. Rev.* **C32**, 721 (1985).
[14] E. F. Redish, D. M. Schneider, *Phys. Lett.* **100B**, 101 (1981).
[15] J. Aichelin, H. Stöcker, *Phys. Lett.* **163B**, 59 (1985).